Available online at www.sciencedirect.com
ScienceDirect
Journal of Sound and Vibration 324 (2009) 209–220
JOURNAL OF SOUND AND VIBRATION
www.elsevier.com/locate/jsvi

Synchronization of coupled self-excited elastic beams

Miguel A. Barrón[a,*], Mihir Sen[b]

[a]Departamento de Materiales, Universidad Autónoma Metropolitana-Azcapotzalco, Av. San Pablo 180, México, D.F. 02200, Mexico
[b]Department of Aerospace and Mechanical Engineering, University of Notre Dame, Notre Dame, IN 46556, USA

Received 20 June 2008; received in revised form 30 January 2009; accepted 2 February 2009
Handling Editor: C.L. Morfey
Available online 12 March 2009

Abstract

The behavior of four coupled self-excited elastic beams is numerically studied using the finite-difference method. Self-excitation is modeled by adding a van der Pol damping term. Coupling based on shared boundary conditions at the roots of the beams is proposed, and the influence of the coupling on the dynamics is analyzed. Time and space correlation coefficients are employed to measure the degree of synchronization among beams. Through the power spectral density, multiple frequencies of the beam tip time series are determined, unveiling the complex nature of the beam motions. Finally, the robustness of the proposed behavior to changes in fluid–structure interaction and the mass of the beams is determined.

1. Introduction

Failures of turbine blades are frequently observed in turbomachinery. There may be many different causes, but an important one is fatigue by vibration [1–3]. Detailed experiments of blade vibration are quite problematic given that installing sensors in compressors or turbine blades during operation is notoriously difficult, and instruments may be intrusive and interfere with machine operation. Noncontact measurement techniques have been proposed [4]; however, frequently they are very expensive or require long installation times. Numerical studies also face considerable difficulties. Not only have many blades to be modeled and computed, but also the fluid flow and its interaction with each one of the blades [5–8].

Unbalanced rotating shafts, such as turbines, that are connected to a common structure have been observed to synchronize [9]. There also exists the definite possibility of the synchronization of the oscillations of turbine blades fixed to a single shaft due to coupling through the fluid or the elasticity of the shaft. We know that a single cantilever beam in the presence of cross-flow exhibits self-excited oscillations due to the interaction between vortex shedding in the wake and the beam itself, so that the oscillations of a group of cantilever beams coupled through a common base may synchronize too. Observation of this phenomenon has not been yet reported, so that it is a strong and timely argument for making the present study.

Recently, the coupling behavior of a shaft–disk–blades system of rotating machinery has been analyzed [10]. The authors employ the energy approach and the assumed-modes method, and identify four types of coupling

*Corresponding author. Tel./fax: +52 55 5318 9474.
E-mail address: bmma@correo.azc.uam.mx (M.A. Barrón).

0022-460X/$ - see front matter © 2009 Elsevier Ltd. All rights reserved.
doi:10.1016/j.jsv.2009.02.007

modes: shaft–blade, shaft–disk–blades, disk–blades, and blade–blade. They focus on the influence of disk flexibility on coupled behavior and report that it strongly affects mode bifurcation and the transition between modes. The collective behavior of vibrating blades have been reported using different techniques: Prony spectral analysis [11], frequency domain with quasilinearization [12], blade-tip timing [13,14], large eddy simulation with computational fluid dynamics [7], complex constraint method [15], linearized Euler analysis [16], theory of beams [17], finite element [18], fluid–structure approach [19], and so on. Unfortunately, in all of the above the issue of synchronization between blades is not addressed, though there is some recognition of synchronization as a cause of rotating machinery malfunction, e.g. voltage flicker problems in wind farms [20].

Considerable progress has been made in the analysis of the synchronization of several, coupled single degree of freedom systems. Woafo and collaborators have studied this problem in a series of papers [21–23]. They looked at the synchronization of a ring of four identical van der Pol oscillators by linearization around the unperturbed limit cycle, and the results have been experimentally corroborated. Also, synchronization of four self-sustained quasilinear electromechanical devices was analyzed using the Floquet theory, though the results are only valid for a small region of parameter space where the values of the self-exciting constants are near zero. Synchronization of four van der Pol oscillators in the strongly nonlinear region has been addressed by the present authors [24], where the existence of two regions with a multiplicity of periodic attractors is reported; the size of these regions strongly depends on the values of the self-exciting and coupling constants. Czolczynski and collaborators [25,26] have reported that chaotic and self-excited oscillators, coupled through an elastic structure, may exhibit periodic full synchronization. The main difference with the present work lies in that they studied the synchronization of oscillators that were of the single degree of freedom type, while oscillators with infinite degrees of freedom are considered here. There are of course several differences when dealing with systems with infinite degrees of freedom, such as the interaction between the modes not only between oscillators but within an oscillator itself. In spite of that, there is much to be learned from the study of finite degrees of freedom systems, and this work can be viewed as an extension of those [21–26].

Given the computational complexity of the complete problem, it is necessary to begin with some simplifications. Let us ignore torsional oscillations and consider a number of cantilever beams exhibiting self-excited bending oscillations due to the presence of cross-flow. Self-excitation can be modeled by a nonlinear damping term in the beam equation to model the fluid–structure interaction. The flow around a cylinder is a common situation in which a cantilevered cylinder, when submerged in a steady flow, begins to oscillate. Strictly speaking, the Navier–Stokes equation should be used for the fluid in conjunction with the equations of elasticity for the structure. We are looking here, however, for a simplified model which will have the elements necessary for self-excitation of the beam, but not be very computationally demanding since a number of these coupled oscillators have to be simultaneously computed. The model must, of necessity, be nonlinear since a linear model can only respond to external excitation but cannot sustain self-excited oscillations. There are many mathematical models of flow–structure interaction which leads to the self-excited oscillations of the structure [27,28]. The van der Pol equation is one that has been used in the literature, though other types of models have also been proposed. Bishop and Hassan [29] have suggested using a van der Pol type oscillator to represent the time-varying forces on a cylinder due to vortex shedding. Lee and collaborators [30] used it for the study of an aeroelastic system possessing limit cycle oscillations. Hartlen and Currie [31] also introduced a van der Pol-based model that captures many of the features seen in experimental results, and which has been subsequently modified and improved [32]. Though single elastic beams have been studied extensively [33–43], nothing could be found on the coupled behavior of several beams. It is expected that coupled self-excited beams present a wide variety of dynamic behavior, in part due to the distributed nature of the beams.

Here the dynamic behavior of four self-excited elastic beams is numerically studied using the finite-difference method. In practice, there may be more than four beams, but four were chosen for analysis because this is the smallest number for which there is at least one beam that is not an immediate neighbor. The results may generalize to a larger number of beams which will be considered for future work. Self-excitation is modeled through a van der Pol term in the elastic beam equation. Coupling based on shared boundary conditions at the roots of the beams is proposed, and the influence of the coupling on the dynamics is analyzed. Time and space correlation coefficients are employed to measure the degree of synchronization among beams. Through a power spectral density analysis, multiple frequencies of the beam tip time series are

determined. The robustness of the proposed coupling to changes in the fluid–structure interaction and mass of beams is studied by introducing detuning parameters in one beam.

2. Mathematical model

The governing equation for the transverse motion of a thin rod or beam of homogeneous section and properties, as shown in Fig. 1, is [44]

$$\frac{\partial^4 y}{\partial x^4} + \frac{1}{a^2}\frac{\partial^2 y}{\partial t^2} = 0, \tag{1}$$

with

$$a^2 = \frac{EI}{\rho A_c}, \tag{2}$$

where x is the distance from the root, $y(x,t)$ is the transverse displacement, t is the time, and E, I, ρ and A_c are Young's modulus, the moment of inertia, the mass density per unit volume, and the cross-sectional area of the beam, respectively. Defining the nondimensional variables $X = x/L$, $Y = y/L$, $\tau = ta/L^2$, where L is the beam length, one gets

$$\frac{\partial Y^4}{\partial X^4} + \frac{\partial Y^2}{\partial \tau^2} = 0. \tag{3}$$

To include the fluid–structure interaction, a van der Pol term

$$\frac{\partial^4 Y}{\partial X^4} + \frac{\partial^2 Y}{\partial \tau^2} + A(Y^2 - 1)\frac{\partial Y}{\partial \tau} = 0, \tag{4}$$

the third from the left, is added to model the self-excited oscillations [29–31].

3. Coupling between beams

We will assume that there are four beams with transverse displacement $Y_i(X,\tau)$, $i = 1,\ldots,4$ so that for each

$$\frac{\partial^4 Y_i}{\partial X^4} + \frac{\partial^2 Y_i}{\partial \tau^2} + A(Y_i^2 - 1)\frac{\partial Y_i}{\partial \tau} = 0. \tag{5}$$

Several ways of coupling between the four beams can be considered. For example, coupling through the entire length of the beams may be present for very large flow Reynolds numbers. For an arrangement such as that shown in Fig. 2, coupling through the roots of the beams, corresponding to transmission of vibrations to the nearest neighbors through the shaft, can be assumed. Each beam is subject to the boundary conditions [44]

$$Y_i = 0 \quad \text{at } X = 0, \tag{6}$$

$$\frac{\partial^2 Y_i}{\partial X^2} = 0 \quad \text{at } X = 1, \tag{7}$$

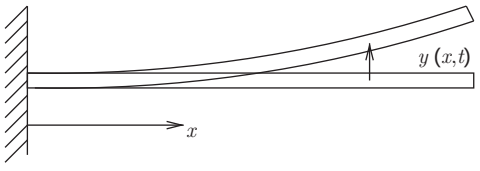

Fig. 1. Geometry of single beam.

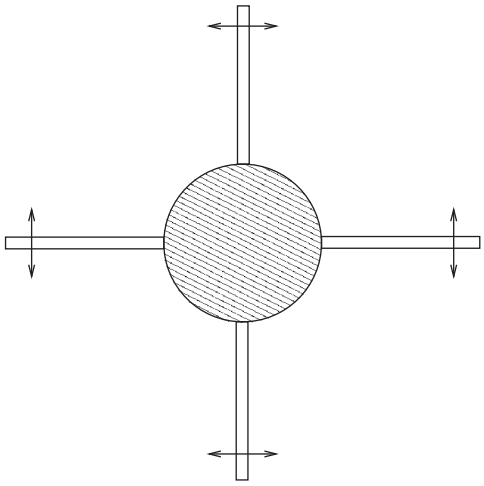

Fig. 2. Four beams on same shaft.

$$\frac{\partial^3 Y_i}{\partial X^3} = 0 \quad \text{at } X = 1. \tag{8}$$

The remaining boundary condition for a *single*, uncoupled beam would be $\partial Y/\partial X = 0$ at $X = 0$. *Multiple* beams, however, are structurally coupled through the shaft to which they are fixed. Since the displacements are zero at the bases of the beams, the coupling must be through the slopes of the beams at that point. The simplest coupling can be assumed to be like a linear torsional spring so the slope at the base of a beam is proportionately affected by its difference with respect to its neighbors. If two beams move together there is no coupling, but if they do not then there is an effect that is proportional to the difference in slopes. Thus we have

$$S_i = K(S_{i-1} + S_{i+1}), \tag{9}$$

where $S_i = \partial Y_i/\partial X$ at $X = 0$. i goes from 1 to 4 in the form of a ring. K is a constant that determines the strength of the coupling; for $K = 0$ the beams are uncoupled. The four conditions (9) should be linearly independent. This can be checked by looking at linear system $\mathbf{KS} = \mathbf{0}$ constructed from Eq. (9), where $\mathbf{S} = [S_1\ S_2\ S_3\ S_4]^{\mathrm{T}}$ and the coupling matrix $\mathbf{K}$ is given by

$$\mathbf{K} = \begin{bmatrix} 1 & -K & 0 & -K \\ -K & 1 & -K & 0 \\ 0 & -K & 1 & -K \\ -K & 0 & -K & 1 \end{bmatrix}. \tag{10}$$

It is seen that

$$\det \mathbf{K} = 1 - 4K^2, \tag{11}$$

so that $\mathbf{K}$ becomes singular for $K = \frac{1}{2}$. The boundary conditions (9) are linearly independent for any other value of K.

4. Numerical solution

The finite-difference method is a simple but powerful tool for solving linear and nonlinear partial differential equations; it has been widely used in the past to solve vibration problems in beams and other bodies [45–49]. In this method the partial derivatives and the boundary conditions are approximated by difference equations, and the resulting simultaneous algebraic equations are numerically solved. The discretization schemes suggested in Ref. [50] for the vibration of beams are applied in an explicit form.

In order to assure stability and convergence in the numerical simulations, the following parameter values are employed in the computer runs: spatial step $\Delta X = 0.005$, time step $\Delta\tau = 10^{-6}$.

Numerical simulations show that for $K > \frac{1}{2}$ the coupled system becomes unstable, so that $K \in [0, \frac{1}{2})$ defines the permitted range of values of the coupling constant. For this nonlinear problem, initial conditions play a crucial role in determining the long-time solutions that are obtained since multiple attractors exist. The transverse positions of the four coupled beams, $Y_i(X,\tau)$, are monitored both in space and time during the computer runs. However, for simplicity the beam tip position is monitored for tracking purposes. This has emerged as a promising method for the detection, measurement and analysis of blade vibrations in rotating bladed assemblies in recent years [51]. In this context, a tracking point located in the tip of the beams is monitored in time in order to characterize lowest-mode attractor corresponding to particular values of the coupling constant and initial condition.

The time correlation coefficient R_{ij}^t [52] is employed to measure the strength and sign of the interdependence between the ith and jth beams. The correlation coefficient indicates the magnitude and direction of a linear relationship between two variables and is defined by

$$R_{ij}^t = \frac{E\{(x_i - \overline{x}_i)(x_j - \overline{x}_j)\}}{\sigma_i \sigma_j}, \tag{12}$$

where $\overline{x}_i$ is the mean of the series x_i, σ_i is its standard deviation, and $E\{\}$ is the expected value. It is known that $R_{ij}^t \in [-1, 1]$, and if the beams i and j have a strong positive correlation, R_{ij}^t is close to $+1$, whereas for a strong negative correlation R_{ij}^t is close to -1. Generally speaking, for our purposes if $|R_{ij}^t| > 0.8$ the correlation is considered *strong*, whereas for $|R_{ij}^t| < 0.5$ the correlation is *weak*; if $0.5 \leqslant |R_{ij}^t| \leqslant 0.8$ the correlation is judged as *average*. In this way, R_{ij}^t is employed as a measure of the degree of time synchronization between two coupled beams: $R_{ij}^t = +1$ indicates perfect in-phase synchronization, $R_{ij}^t = -1$ is perfect anti-phase synchronization, and $R_{ij}^t = 0$ means complete desynchronization. Sometimes a subset of the four beams will behave in one way, an effect that will be referred to here as *clustering*. A spatial correlation, R_{ij}^x, is also calculated.

The power spectral density is used to characterize the complex periodic behavior of the beam tip. It shows how the power or energy of a time series is distributed with frequency, and is defined as the Fourier transform of the autocorrelation sequence of the time series [53,54]. As is shown later, for small values of K a quasiperiodic amplitude-modulated oscillation of the beam tips is obtained, in which case the power spectral density is a very useful tool to find the frequencies of the main vibration modes of a particular attractor.

5. Results

Numerical simulation were carried out for $A = 5.0$ and $K = 0.01, 0.1, 0.2, 0.3, 0.4, 0.45$ using the initial conditions shown in Table 1. In order to avoid transient effects and assure a steady dynamic response, the integration time was taken to be 200 time units, which represents around 3500 cycles of the lowest detected frequency. The beam position, $Y_i(X,\tau)$, and beam tip position, $Y_i(1,\tau)$, were recorded at every 0.1 and 0.0001 time units, respectively.

For values of the coupling constant near zero the dynamic behavior of the beam tips is very complex, as can be appreciated in Fig. 3 and Table 2 for $K = 0.01$. In addition to the time and spatial correlation coefficients, f_i and A_i are the frequency and amplitude of the ith beam tip, respectively. When a value of f_i is in *italics*, it corresponds to the main frequency of a quasiperiodic attractor whose multiple frequencies were obtained through the power spectrum. For IC1, Fig. 3(a) shows a perfect amplitude-modulated anti-phase cluster

Table 1
Initial conditions (IC) for numerical simulations.

IC	Y_1	$\partial Y_1/\partial\tau$	Y_2	$\partial Y_2/\partial\tau$	Y_3	$\partial Y_3/\partial\tau$	Y_4	$\partial Y_4/\partial\tau$
1	1	0	0	1	−1	1	1	1
2	1	1	1	0	−1	0	1	−1
3	2	0	−2	2	0	−3	4	−1
4	2	2	3	3	4	4	4	1

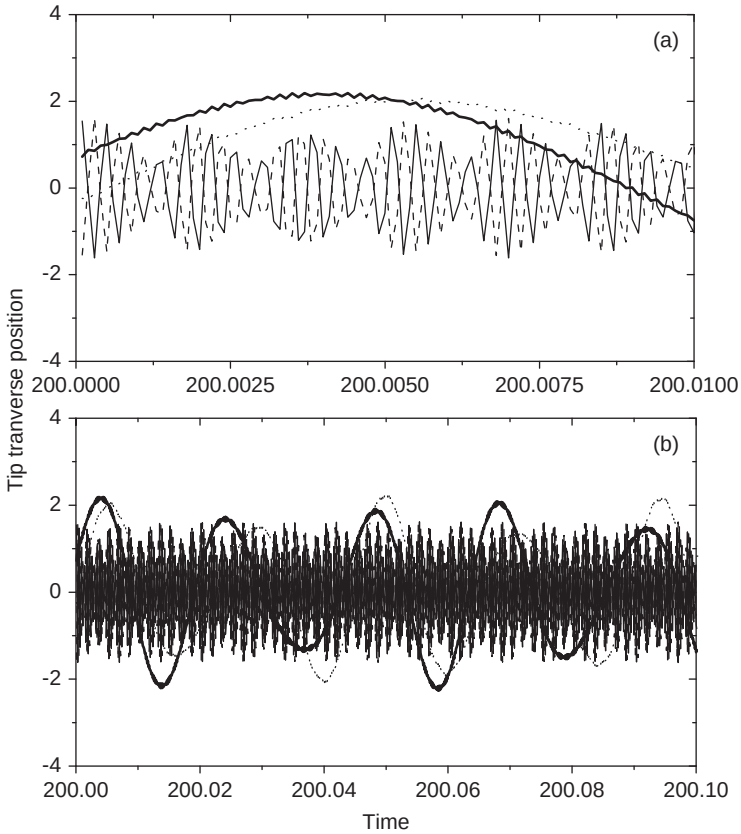

Fig. 3. Time series of tip transverse positions for coupled beams with $K = 0.01$ and initial condition 1 of Table 1. (a) Time lapse of 0.01; (b) time lapse of 0.1. First beam: thick line; second beam: thin line; third beam: dotted line; fourth beam: dashed line.

between the tips of the second and fourth beams with $R^t_{24} = -1$ and a main frequency of 2386.71 Hz as shown in Table 2. Fig. 3(b) exhibits the dynamic behavior of the first and third beam tips. In accordance to Table 2 the main frequency is 45.79 Hz for both tips (the unit Hz is used in a nondimensional sense), but in this case $R^t_{24} = 0.6945$, which suggests an average correlation rather than a strong one. This apparent discrepancy is due to the presence of the frequency component 65.29 Hz for the first beam, which prevents full synchronization. The presence of multiple amplitudes corroborates too the complex nature of dynamic tip behavior; for instance for IC1 the tips of the first and third beams exhibit two amplitudes, 1.36 and 1.28, whereas the second and fourth beams have three different amplitudes, 0.60, 1.52 and 1.63.

Table 2 shows that for $K = 0.01$ and IC2, $R^t_{13} = -0.8693$ and $R^t_{24} = 0.9627$; this implies a strong negative correlation and a strong positive correlation between the tip movements of the first and third beams, and the second and fourth beams, respectively. Numerical simulations show that time and spatial correlation coefficients for the same beams do not always agree between them, i.e. for a given value and sign of the time correlation coefficient for certain pair of beams it is not necessary that the spatial correlation coefficient be of the same order of magnitude and sign. For instance, for IC2 Table 2 indicates that for the first and third beams $R^t_{13} = -0.8693$, whereas $R^x_{13} = 0.3943$. This means that while the tips are in an anti-phase synchronization state, the beam positions may present weak or null synchronization. For $K = 0.01$ and IC3, Table 2 shows that $R^t_{13} = -0.9879$, $R^t_{24} = -0.9860$, $R^t_{13} = -0.9997$ and $R^x_{24} = -0.9573$. This indicates the presence of two clusters, one between the first and third beams, and another between the second and fourth beams; both clusters exhibit strong anti-phase synchronization in time as well as space. Also, $R^x_{14} = 0.9769$ and $R^x_{23} = 0.8848$ indicate strong positive spatial synchronization between first and fourth beams, and second and third beams, respectively. All beams present two frequencies, 1185.69 and 4185.69 Hz, and two amplitudes, the 1185.69 Hz frequency being dominant with the highest power spectral value. From the four initial conditions

Table 2
Parameters of attractors for initial conditions of Table 1, and $K = 0.01$.

Parameter	IC1	IC2	IC3	IC4
R^t_{12}	0.0000	−0.3383	−0.6151	0.6693
R^t_{13}	0.6945	−0.8693	−0.9879	−0.3800
R^t_{14}	0.0001	−0.1046	0.6320	0.0061
R^t_{23}	−0.0001	0.6318	0.6243	−0.8019
R^t_{24}	−1.0000	0.9627	−0.9860	−0.0079
R^t_{34}	0.0001	0.4388	−0.6387	0.0071
R^x_{12}	−0.0012	0.1999	−0.8735	−0.8295
R^x_{13}	0.5013	0.3943	−0.9997	−0.7066
R^x_{14}	0.0013	0.0478	0.9769	0.1705
R^x_{23}	−0.0018	0.9168	0.8848	0.2800
R^x_{24}	−1.0000	0.9737	−0.9573	−0.0740
R^x_{34}	0.0007	0.8131	−0.9817	−0.0234
f_1	*45.79*, 65.29	33.55	*1185.69*, 4185.69	41.47
f_2	*2386.71*, 2987.22	33.55	*1185.69*, 4185.69	41.47
f_3	45.79	33.55	*1185.69*, 4185.69	41.47
f_4	*2386.71*, 2987.22	33.55	*1185.69*, 4185.69	17.66
A_1	1.36, 2.28	1.68, 2.46	1.62, 1.73	1.61, 2.25
A_2	0.60, 1.52, 1.63	1.62, 2.46	1.62, 1.73	1.82, 2.17
A_3	1.36, 2.28	1.67, 2.44	1.62, 1.73	1.82, 2.17
A_4	0.60, 1.52, 1.63	1.69, 2.47	1.62, 1.73	2.42, 2.90

Frequency values in *italics* represent main frequency for those attractors with multiple periods.

Table 3
Parameters of attractors for initial conditions of Table 1, and $K = 0.4$.

Parameter	IC1	IC2	IC3	IC4
R^t_{12}	−0.0329	−0.8687	0.0143	0.6295
R^t_{13}	−0.9965	−0.8888	−0.0046	1.0000
R^t_{14}	0.0621	−0.8767	0.0101	0.6295
R^t_{23}	−0.0466	0.8988	−0.0115	0.6295
R^t_{24}	0.9950	0.9085	0.0064	1.0000
R^t_{34}	−0.1411	0.8861	0.0147	0.6295
R^x_{12}	0.8162	−0.9945	−0.1181	−0.7960
R^x_{13}	0.8547	0.8219	−0.9790	1.0000
R^x_{14}	0.8204	−0.9869	0.0814	−0.7960
R^x_{23}	0.9065	−0.8703	0.0837	−0.7960
R^x_{24}	0.9815	0.9777	−0.8862	1.0000
R^x_{34}	0.9664	−0.7722	−0.0508	−0.7960
f_1	17.66	32.38	17.66	46.89, 81.52, *285.82*
f_2	17.66	32.38	27.55	46.89, 81.52, *285.82*
f_3	17.66	32.38	17.66	46.89, 81.52, *285.82*
f_4	17.66	32.96	27.55	46.89, 81.52, *285.82*
A_1	3.48	2.83	3.08	0.31, 3.57
A_2	3.47	2.70	2.35	0.31, 3.61
A_3	3.50	2.44	3.08	0.31, 3.57
A_4	3.47	2.72	2.34	0.31, 3.61

Frequency values in *italics* represent main frequency for those attractors with multiple periods.

considered, it is IC3 which, in accordance to Table 2, gives the highest absolute values of the spatial correlation coefficients in spite of the small value of the coupling constant. For $K = 0.01$ and IC4, just two values of the correlation coefficients in Table 2 indicate significant synchronization: $R^t_{23} = -0.8019$ and

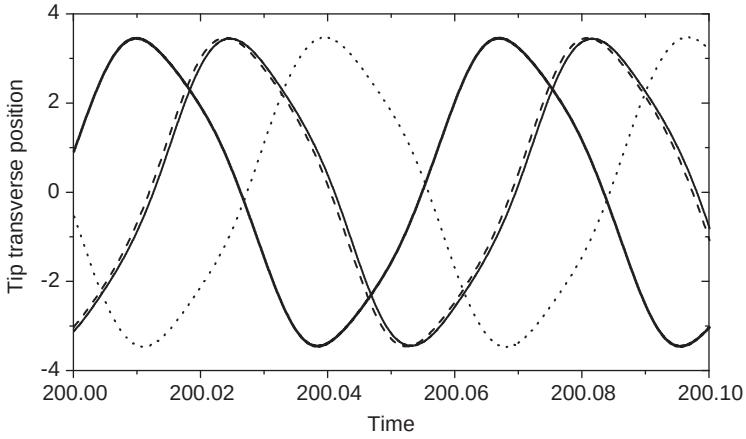

Fig. 4. Time series of tip transverse position for coupled beams with $K = 0.4$ and initial condition 1 of Table 1. First beam: thick line; second beam: thin line; third beam: dotted line; fourth beam: dashed line.

$R^x_{12} = -0.8295$; the first one implies a strong time anti-phase synchronization between the second and third beams, and the second a strong spatial anti-phase synchronization between the first and second beams.

Table 3 summarizes the results for $K = 0.4$. In Fig. 4 the time series of the beam tips for $K = 0.4$ and IC1 are shown. A cluster in anti-phase synchronization is observed between the tip movements of the first and third beams, and another in in-phase synchronization is appreciated between the tip movements of the second and fourth beams. This is corroborated through the values of the corresponding time correlation coefficients, $R^t_{13} = -0.9965$ and $R^t_{24} = 0.9950$, shown in Table 3. Both clusters have 90° phase-shift between them. For $K = 0.4$, IC2 gives a strong correlation, positive or negative, between all beams, with the exception of the average negative spatial correlation between third and fourth beams indicated by $R^x_{34} = -0.7722$. In accordance to Table 3, IC3 yields just two significant correlation coefficients: $R^x_{13} = -0.9790$ and $R^x_{24} = -0.8862$; these values suggest strong negative correlations, or significant anti-phase synchronization, between the first and third beams, and the second and fourth beams, respectively. For $K = 0.4$ and IC4, the values $R^x_{13} = R^t_{13} = 1$ indicate perfect in-phase synchronization, both in time and space, between first and third beams. However, among the four initial conditions considered for $K = 0.4$, it is IC4 which yields an attractor with multiple frequencies and amplitudes. In this case it is the frequency of 285.82 Hz which is the highest and the dominant frequency of the attractor.

The power spectral densities for the position of the first beam tip using IC1 for the values of the coupling constant considered are shown in Fig. 5. Two or more significant power peaks are observed for $K \leqslant 0.3$ in Fig. 5(a)–(d). Each peak corresponds to a component frequency, and the highest peak represents the main or dominant frequency. The case of $K = 0.1$ presents the higher number of frequencies. One can note that as K is increased, the multiplicity of peaks in the spectrum tends to disappear. This means that the tip movements become less complex, with just a single frequency and a single amplitude, as can be verified comparing Tables 2 and 3. It can also be observed that the frequency associated with the highest peak of the power spectrum tends to decrease for $K \leqslant 0.3$; therefore the main frequency of each tip attractor decreases too, as in Fig. 6. This figure also shows a significant increment in the main frequency of the beam tip attractors for $K = 0.4$ for first, third and fourth beams. For the second beam the increment in frequency occurs for $K = 0.2$. With the exception of the second beam, the frequency decreases for $K > 0.4$, may be due to the fact that the coupling constant is approaching its critical value of $K = \frac{1}{2}$ at which the coupling matrix $\mathbf{K}$ becomes singular.

6. Robustness

It is interesting to study the robustness of the coupled beam behavior to perturbations in the fluid–structure interaction and the mass of the beams. In this work the fluid–structure interaction is modeled through a damping term of the van der Pol type with a certain constant. Given that beam density is included in the a^2 of

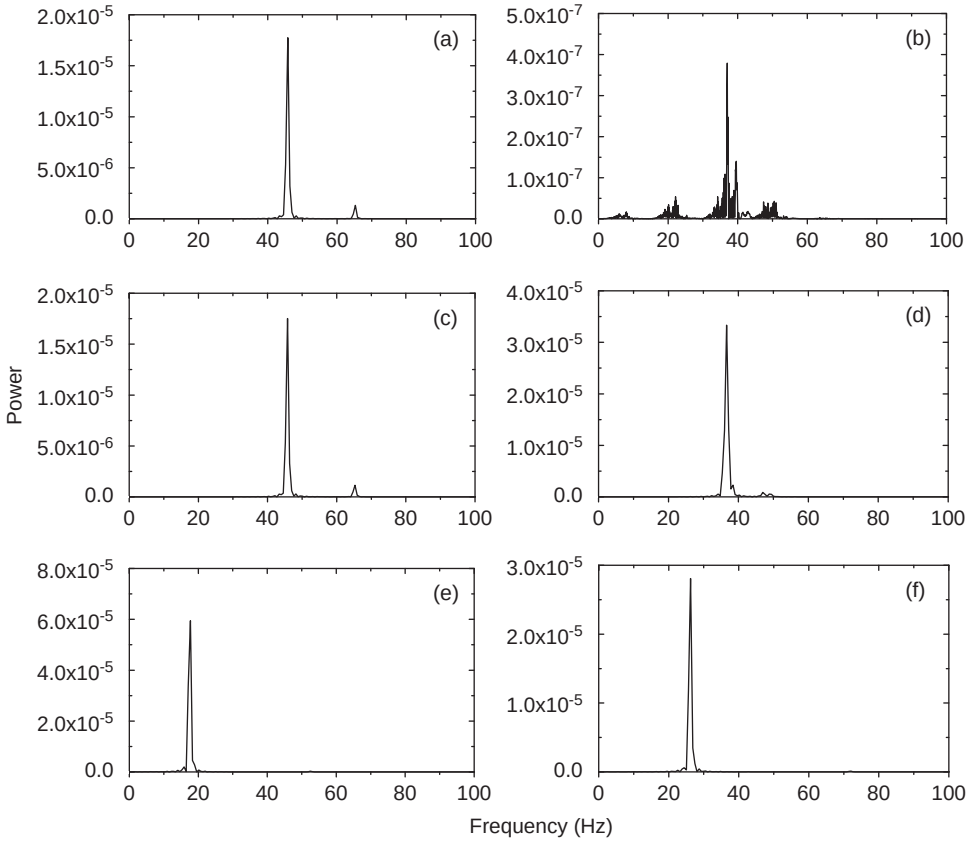

Fig. 5. Power spectral density for time series of first beam tip. Initial condition 1 of Table 1. (a) $K = 0.01$, (b) $K = 0.1$, (c) $K = 0.2$, (d) $K = 0.3$, (e) $K = 0.4$, (f) $K = 0.45$.

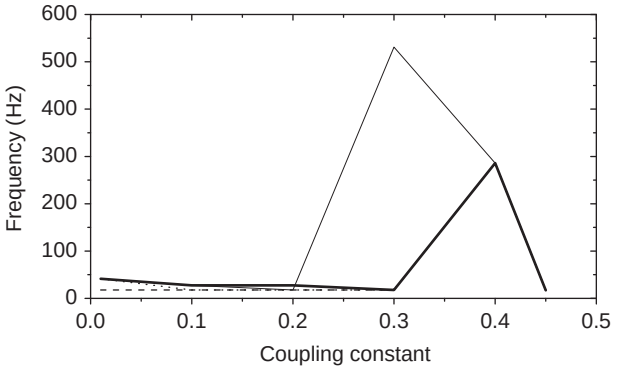

Fig. 6. Main frequency of beam tip attractor as function of coupling constant. First beam: thick line; second beam: thin line; third beam: dotted line; fourth beam: dashed line.

Eq. (2), beam mass can be modeled through the coefficient of the second-order time derivative of Eq. (5). With this in mind, it is possible to rewrite it as

$$\frac{\partial^4 Y_i}{\partial X^4} + C_i \frac{\partial^2 Y_i}{\partial \tau^2} + A_i^*(Y_i^2 - 1)\frac{\partial Y_i}{\partial \tau} = 0. \tag{13}$$

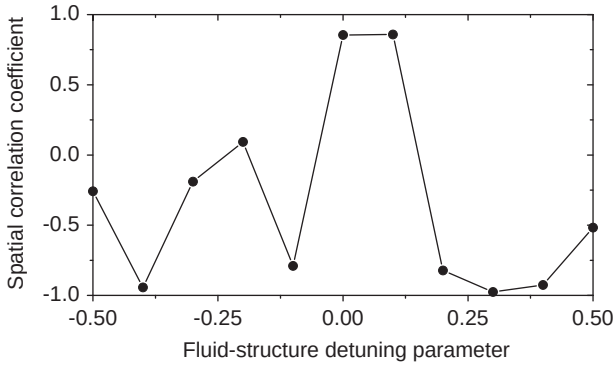

Fig. 7. Spatial correlation coefficient between first and third beams as function of fluid–structure detuning parameter, h_f.

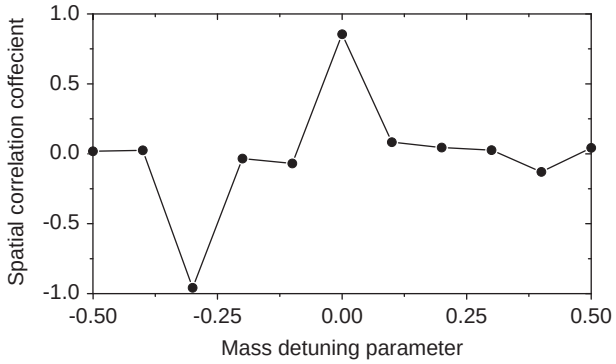

Fig. 8. Spatial correlation coefficient between first and third beams as function of mass detuning parameter, h_m.

In the computer simulations only the first beam is perturbed, so that $C_1 = 1 + h_m$, and $A_1^* = A(1 + h_f)$, where h_m and h_f are the mass and the fluid–structure detuning parameters, respectively. Using $K = 0.4$ and IC1 as the reference state, Table 3 shows that this combination of coupling constant and initial condition gives $R_{13}^x = 0.8547$, the spatial correlation coefficient between the first and third beams. Fig. 7 shows the influence of the fluid–structure detuning parameter on R_{13}^x. A narrow band of robustness can be appreciated for $h_f \in [0, 0.1]$; in this region synchronization between first and third beams is preserved. For $h_f \in [0.2, 0.4]$ in-phase synchronization becomes anti-phase synchronization, as is suggested by values of R_{13}^x around -1. For $h_f \in [-0.5, -0.1]$ a transition region is present in which the coupling between the first and third beams is changing from desynchronization to anti-phase synchronization.

Fig. 8 shows the effect of the mass detuning parameter on R_{13}^x. With the exception of $h_m = -0.3$, $R_{13}^x = 0$ for the majority of values of h_m. This means that the coupling between the first and third beams becomes fully desynchronized for changes in the mass of the beams. Comparing Figs. 7 and 8, it becomes evident that, under the proposed coupling, synchronization of the four coupled beams is more sensitive to changes in the mass of the beams compared to changes in the fluid–structure interaction.

7. Conclusions

Synchronization of four coupled elastic beams has been numerically computed. The simulations show that for values of the coupling constant near zero the motions of the beam tips, and therefore the motions of the entire beam, are very complex and exhibit multiple frequencies and amplitudes. As the coupling constant is increased the motion becomes more regular and finally exhibits a single frequency and amplitude. Synchronization among beams, which is quantified through correlation coefficients, is enhanced as the

coupling constant is increased. Sometimes time and space correlation coefficients are not in agreement, which can be explained by the elastic nature of the beams. Finally, the synchronized behavior of the coupled system shows more robustness to changes in the fluid–structure interaction than to changes in the mass of the beams.

Acknowledgments

This work was done while Miguel A. Barrón was on sabbatical leave from the *Universidad Autónoma Metropolitana-Azcapotzalco* (*UAM-A*) and visiting the *University of Notre Dame*. He gratefully acknowledges financial support from the *Programa de Apoyo a Estancias Sabáticas de Investigación* of the *UAM-A*.

References

[1] G. Tsai, Rotating vibration behavior of the turbine blades with different groups of blades, *Journal of Sound and Vibration* 271 (2004) 547–575.
[2] Y. Lau, R. Leung, R. So, Vortex-induced vibration effect on fatigue life estimate of turbine blades, *Journal of Sound and Vibration* 307 (2006) 698–719.
[3] Z. Mazur, R. Garcia-Illescas, J. Aguirre-Romano, N. Perez-Rodriguez, Steam turbine blade failure analysis, *Engineering Failure Analysis* 15 (2008) 129–141.
[4] P. Beauseroy, R. Lengelle, Nonintrusive turbomachine blade vibration measurement system, *Mechanical Systems and Signal Processing* 21 (2007) 1717–1738.
[5] Z. Jaworski, K. Dyster, A. Nienow, The effect of size, location and pumping direction of pitched blade turbine impellers on flow patterns: LDA measurements and CFD predictions, *Chemical Engineering Research & Design* 79 (A8) (2001) 887–894.
[6] A. Datta, J. Sitaraman, I. Chopra, J. Baeder, CFD/CSD prediction of rotor vibratory loads in high-speed flight, *Journal of Aircraft* 43 (6) (2006) 1698–1709.
[7] Y. Jiang, S. Yoshimura, R. Imai, H. Katsura, T. Yoshida, C. Kato, Quantitative evaluation of flow-induced structural vibration and noise in turbomachinery by full-scale weakly coupled simulation, *Journal of Fluids and Structures* 23 (4) (2007) 531–544.
[8] C. Rodriguez, E. Egusquiza, I. Santos, Frequencies in the vibration induced by the rotor stator interaction in a centrifugal pump turbine, *ASME Journal of Fluids Engineering* 129 (11) (2007) 1428–1435.
[9] M. Dimentberg, E. Cobb, J. Mensching, Self-synchronization of transient rotations in multiple shaft systems, *Journal of Vibration and Control* 7 (2001) 221–232.
[10] C. Yang, S. Huang, The influence of disk's flexibility on coupling vibration of shaft–disk–blades systems, *Journal of Sound and Vibration* 301 (2007) 1–17.
[11] O. Balakshin, B. Kukharenko, A. Khorikov, Identification of turbine blade flutter, *Journal of Machinery Manufacture and Reliability* 37 (2008) 16–20.
[12] E. Cigeroglu, H. Ozguven, Nonlinear vibration analysis of bladed disks with dry friction dampers, *Journal of Sound and Vibration* 295 (2006) 1028–1043.
[13] G. Dimitriadis, I. Carrington, J. Wright, J. Cooper, Blade-tip timing measurement of synchronous vibrations of rotating bladed assemblies, *Mechanical Systems and Signal Processing* 16 (2002) 599–622.
[14] C. Lawson, P. Ivey, Turbomachinery blade vibration amplitude measurement through tip timing with capacitance tip clearance probes, *Sensors and Actuators A* 118 (2005) 14–24.
[15] J. Li, S. Lie, Z. Cen, Numerical analysis of dynamic behavior of steam turbine blade group, *Finite Elements in Analysis and Design* 35 (2000) 337–348.
[16] J. Panovsky, R. Kielb, A design method to prevent low pressure turbine blade flutter, *Journal of Engineering for Gas Turbines and Power* 122 (2000) 89–98.
[17] G. Pisarenko, Y. Vorobev, Issues on simulation of turbomachine blade vibration, *Strength of Materials* 32 (2000) 487–489.
[18] J. Rao, A. Saldanha, Turbomachine blade damping, *Journal of Sound and Vibration* 262 (2003) 731–738.
[19] R. Rzadkowski, V. Gnesin, 3-D inviscid self-excited vibrations of a blade row in the last stage turbine, *Journal of Fluids and Structures* 23 (2007) 858–873.
[20] N. Katayama, G. Takata, M. Miyake, T. Nanahara, Theoretical study on synchronization phenomena of wind turbines in a wind farm, *Electrical Engineering in Japan* 155 (2006) 1123–1131.
[21] P. Woafo, H. Kadji, Synchronization states in a ring of mutually self-sustained electrical oscillators, *Physical Review E* 69 (2004) 046206.
[22] B. Nana, P. Woafo, Synchronization of a ring of mutually coupled van der Pol oscillators: theory and experiment, *Physical Review E* 74 (2006) 046213.
[23] R. Yamapi, P. Woafo, Synchronized states in a ring of four mutually coupled self-sustained electromechanical devices, *Communications in Nonlinear Science* 11 (2006) 186–202.
[24] M. Barrón, M. Sen, Synchronization of four coupled van der Pol oscillators, *Nonlinear Dynamics*, to be published.
[25] K. Czolczynski, T. Kapitaniak, P. Perlikowski, A. Stefanski, Periodization of Duffing oscillators suspended on elastic structure: mechanical explanation, *Chaos, Soliton and Fractals* 32 (2007) 920–926.

[26] K. Czolczynski, P. Perlikowski, A. Stefanski, T. Kapitaniak, Synchronization of self-excited oscillators suspended on elastic structure, *Chaos, Soliton and Fractals* 32 (2007) 937–943.
[27] P. Hemon, An improvement of the time delayed quasi-steady model for the oscillations of circular cylinders in cross-flow, *Journal of Fluid and Structures* 13 (1999) 291–307.
[28] R. Gabbai, H. Benaroya, An overview of modeling and experiments of vortex-induced vibration of circular cylinders, *Journal of Sound and Vibration* 282 (2005) 575–616.
[29] R. Bishop, A. Hassan, The lift and drag forces on a circular cylinder in a flowing fluid, *Proceedings of the Royal Society Series A* 277 (1963) 32–50.
[30] Y. Lee, A. Vakakis, L. Bergman, D. McFarland, Suppression of limit cycle oscillations in the van der Pol oscillator by means of passive non-linear energy sinks, *Structural Control and Health Monitoring* 13 (2006) 41–75.
[31] R. Hartlen, I. Currie, Lift-oscillator model of vortex induced vibration, *Journal of the Engineering Mechanics* 96 (1970) 577–591.
[32] R. Skop, O. Griffin, A model for the vortex-excited resonant response of bluff cylinders, *Journal of Sound and Vibration* 27 (1973) 225–233.
[33] M. Abu-Hilal, Forced vibration of Euler–Bernoulli beams by means of dynamic Green functions, *Journal of Sound and Vibration* 267 (2003) 191–207.
[34] S. Algazin, Numerical study of free oscillations of a beam with oscillators, *Journal of Applied Mechanics and Technical Physics* 47 (2006) 433–438.
[35] K. Avramov, Bifurcations of parametric oscillations of beams with three equilibria, *Acta Mechanica* 164 (2003) 115–138.
[36] J. Claeyssen, R. Soder, A dynamical basis for computing the modes of Euler–Bernoulli and Timoshenko beams, *Journal of Sound and Vibration* 259 (2003) 986–990.
[37] G. Kostin, V. Saurin, An asymptotic approach to the problem of the free oscillations of a beam, *Journal of Applied Mathematics and Mechanics* 71 (2007) 611–621.
[38] G. Kostin, V. Saurin, Free beam oscillations, *Doklady Physics* 51 (2006) 680–684.
[39] C. Kwuimy, B. Nbendjo, P. Woafo, Optimization of electromechanical control of beam dynamics: analytical method and finite differences simulation, *Journal of Sound and Vibration* 298 (2006) 180–193.
[40] J. Liu, Free vibrations for an asymmetric beam equation, *Nonlinear Analysis* 51 (2002) 487–497.
[41] Y. Tang, Numerical evaluation of uniform beam modes, *Journal of Engineering Mechanics* (2003) 1475–1477.
[42] X. Wang, R. So, Y. Liu, Flow-induced vibration of an Euler–Bernoulli beam, *Journal of Sound and Vibration* 243 (2001) 241–268.
[43] A. Yanmeni, R. Tchoukuegno, P. Woafo, Non-linear dynamics of an elastic beam under moving loads, *Journal of Sound and Vibration* 273 (2004) 1101–1108.
[44] K. Graff, *Wave Motion in Elastic Solids*, Ohio State University Press, Belfast, Ireland, 1975.
[45] A. Kelkar, D. Pai, Finite element and finite difference analysis of the nonlinear flexure of cantilever beam, *Mathematical Modelling and Scientific Computing* 2 (1993) 1159–1164.
[46] M. Arad, A. Yakhot, G. Ben-Dor, A highly accurate numerical solution of a biharmonic equation, *Numerical Methods for Partial Differential Equations* 13 (1997) 375–391.
[47] M. Akanda, S. Ahmed, M. Khan, M. Uddin, A finite-difference scheme for mixed boundary value problems of arbitrary-shaped elastic bodies, *Advances in Engineering Software* 31 (2000) 173–184.
[48] S. Choo, S. Chung, Finite difference approximate solutions for the strongly damped extensible beam equations, *Applied Mathematics and Computation* 112 (2000) 11–32.
[49] G. Chen, Z. Li, P. Lin, A fast finite difference method for biharmonic equations on irregular domains and its application to an incompressible Stokes flow, *Advances in Computational Mathematics* 29 (2008) 113–133.
[50] W. Thomson, *Theory of Vibration with Applications*, Prentice-Hall, Englewood Cliffs, NJ, 1981.
[51] S. Heath, M. Imregun, A survey of blade tip-timing measurement techniques for turbomachinery vibration, *Journal of Engineering for Gas Turbines and Power* 120 (1998) 784–791.
[52] J. Bendat, A. Piersol, *Engineering Applications of Correlation and Spectral Analysis*, Wiley, New York, NY, 1980.
[53] R. Howard, *Principles of Random Signal Analysis and Low Noise Design: The Power Spectral Density and its Applications*, Wiley, New York, NY, 2002.
[54] F. Rudinger, S. Krenk, Spectral density of an oscillator with power law damping excited by white noise, *Journal of Sound and Vibration* 261 (2003) 365–371.